

## Aptamer-Conjugated Covalent-Organic Framework Nanochannels for Selective and Sensitive Detection of Aflatoxin B1

Shi-Lun Li, Zhu-Ying Yan, Hai-Long Qian, Shu-Ting Xu, and Xiu-Ping Yan\*

Cite This: *Anal. Chem.* 2024, 96, 17370–17376

Read Online

ACCESS |



Metrics &amp; More

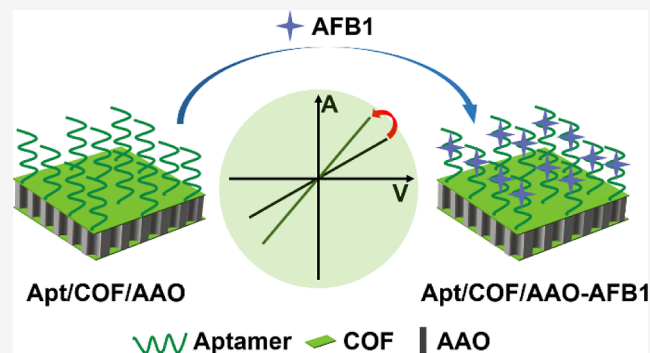


Article Recommendations



Supporting Information

**ABSTRACT:** Sensitive and selective detection of trace aflatoxin B1 (AFB1) in foods is of great importance to guarantee food safety and quality but still challenging because of its trace amount and the interference from the complex food matrix. Here, we report the integration of aptamer (Apt) and an ordered 2D covalent organic framework (COF) to solid-state anodic aluminum oxide (AAO) nanochannels (Apt/COF/AAO) for selective and sensitive detection of trace AFB1. The high specificity of Apt for AFB1 led to a selective change in the surface charge of Apt/COF/AAO and in turn the current change of the nanochannel, permitting the selective and sensitive determination of trace AFB1 in complex food samples. The developed nanofluidic sensor gave a wide linear range (1–500 pg mL<sup>-1</sup>), low detection limit (0.11 pg mL<sup>-1</sup>), and good precision (relative standard deviation of 1.5% for 11 replicate determinations of 100 pg mL<sup>-1</sup>). In addition, the developed sensor was successfully used for the detection of AFB1 in food samples with the recovery of 86.9%–102.5%. The coupling of Apt-conjugated 2D COF with an AAO nanochannel provides a promising way for sensitive and selective determination of food contaminants in complex samples.



## INTRODUCTION

Aflatoxin B1 (AFB1) is listed as Group 1 carcinogen by the International Agency for Research in Cancer.<sup>1–4</sup> AFB1 not only infects a major number of products, including peanuts, corn, grains, wheat, and dried fruits.<sup>5,6</sup> AFB1 could accumulate in the human liver once it invades food chain, eventually leading to chronic liver damage and even death.<sup>7–9</sup> Countries and organizations around the world have established stringent regulatory limits for AFB1 in a range of products.<sup>10,11</sup> To ensure food safety, it is crucial to establish highly sensitive and selective methods to detect trace AFB1 to ensure the safety of food.

Several techniques have been used to determine AFB1 in food, including high-performance liquid chromatography,<sup>12,13</sup> liquid chromatography-tandem mass spectrometry,<sup>14,15</sup> and enzyme-linked immunosorbent assay.<sup>16,17</sup> While these techniques demonstrate high sensitivity and selectivity, they typically necessitate the use of sophisticated instrumentation, as well as complex and time-consuming procedures.

Nanofluidic technologies present novel avenues for ultra-sensitive detection. The confined space allows for a significant improvement in the interaction opportunity between the analyte and the probe for efficacious capture and signal amplification of the target molecule, markedly enhancing the sensitivity and accuracy.<sup>18–21</sup> Biomimetic solid-state nanochannels possess tailorable surface property, chemical and mechanical stability, and controllable channel shape,<sup>22</sup> offering

wide applications in diverse fields,<sup>23</sup> especially in chemical and biological sensing.<sup>24,25</sup> Owing to nanoconfined space-induced target enriching effect, nanochannel sensing systems are promising for sensitive detection of various contaminants in foods,<sup>26</sup> such as ochratoxins A (OTA),<sup>27</sup> formaldehyde,<sup>28</sup> chloramphenicol,<sup>29</sup> mercury,<sup>30</sup> and so on.

Two-dimensional covalent organic frameworks (2D COFs) have picked up significant interest due to their large specific area, abundant hydrogen bonding sites, and intrinsic and highly ordered nanochannels.<sup>31,32</sup> The highly ordered structure and regular pore arrangement of 2D COFs facilitate highly selective detection by interaction with specific analytes, making them excellent for molecular recognition. Their inherent ordered channels not only provide abundant interfacial effects but also further enhance the selectivity of the sensor through the ion-selective permeability in their nanofluidic channels, having them promising in nanofluidic sensing systems.<sup>33–35</sup> Furthermore, the ordered nanochannel structure of 2D COFs introduces more active sites into the sensing process and

**Received:** August 3, 2024  
**Revised:** October 8, 2024  
**Accepted:** October 9, 2024  
**Published:** October 18, 2024



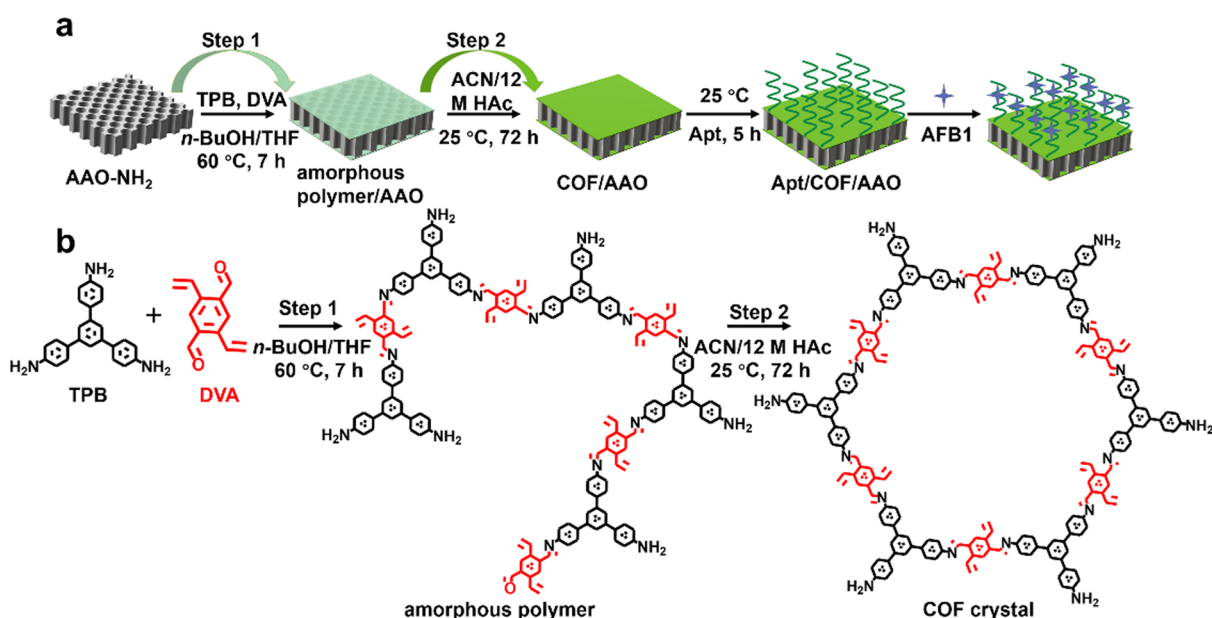


**Figure 1.** (a) Schematic diagram of the Apt/COF/AAO nanofluidic sensor for detection of trace AFB1; (b) illustration for the preparation of the COF crystal through the two-step method.

establishes highly efficient mass-transfer pathways to significantly improve the sensitivity of sensor.<sup>36,37</sup> Consequently, COF-modified nanochannels are considered as kinds of advanced nanofluidic sensors due to their high sensitivity and selectivity.<sup>38–41</sup>

Aptamer (Apt) is a kind of synthetic acceptor and widely applied for the determination of food contaminants owing to its high selectivity, low cost, and stability.<sup>42–45</sup> Integrating Apt into COFs would give rise to the synergetic merits of the porous structure of COFs and the specific recognition ability of aptamers to achieve efficient and specific capture of targets, enabling the precise determination of food contaminants in complex matrices. However, the integration of Apt and COF-modified nanochannels for detecting trace AFB1 in real samples has been unexplored so far.

In this work, we report the facile integration of the specific recognition capability of Apt, the unique porous structure of 2D COF and an anodic aluminum oxide (AAO) nanochannel to design a nanofluidic sensor for selective and sensitive determination of AFB1 in food samples. The imine-bonded 2D COF was grafted on the nanochannels of AAO to yield a COF-functionalized AAO (COF/AAO). The Apt of AFB1 was then conjugated in situ to the COF layer to give Apt-functionalized COF/AAO (Apt/COF/AAO). The strong specific affinity of Apt to AFB1 as well as the 2D COF with highly ordered channels gave the developed Apt/COF/AAO nanofluidic sensor significant potential for selective and sensitive determination of AFB1 in food samples. This work shows the immense potential of Apt and 2D COF-integrated nanofluidic sensors for sensitive and selective detection of hazardous targets in complex food samples.

## EXPERIMENTAL SECTION

**Materials and Chemicals.** Ultrapure water was supplied by Wahaha Co. (Hangzhou, China). 3-Aminopropyltriethoxysilane and *n*-butyl alcohol (*n*-BuOH) were obtained from Aladdin Chemistry Co. (Shanghai, China). (Hydroxymethyl)-methyl aminomethane (Tris, 99%), glacial acetic acid (HAc),

tetrahydrofuran (THF), and acetonitrile (ACN) were purchased from Sinopharm (Shanghai, China). 1,3,5-Tris (4-aminophenyl)benzene (TPB) and 2,5-divinylterephthalaldehyde (DVA) were purchased from Jilin Chinese Academy of Sciences-Yan sheng Technology Co. Ltd. (Changchun, China). The standard solutions for AFB1, aflatoxin B2 (AFB2), aflatoxin G2 (AFG2), zearalenone (ZEN), deoxynivalenol (DON), and OTA were purchased from Anpel Laboratory Technologies Co. (Shanghai, China). Aldehyde group-functionalized aflatoxin B1 aptamer chain with a sequence of CHO -5'-GTT GGG CAC GTG TTG CTC CTC TGT GTC TCG TGC CCT TCG CTA GGC CCA CA-3' was obtained from Sangon (Shanghai, China). AAO film (pore diameter,  $30 \pm 5$  nm; thickness,  $60 \pm 5$   $\mu$ m; pore density, ca.  $2.8 \times 10^{10}$  cm<sup>-2</sup>) was purchased from PuYuan Nanotechnology Co. (Hefei, China). Certified wheat reference material (A299714) was provided by Aladdin Chemistry Co. (Shanghai, China).

**Apparatus.** Zeta potentials were measured on a Nano ZS Zetasizer with a 633 nm He–Ne laser (Malvern, U.K.). X-ray photoelectron spectroscopy (XPS) analyses were performed on an Axis Supra system (Kratos, U.K.). Other instruments for the characterization of materials are described in the [Supporting Information](#).

A laboratory-made nanochannel analysis system was used to measure the ion currents. The system consists of a flow system including two polytetrafluoroethylene flow cells, a 2450 SourceMeter (Keithley, US) and a data acquisition system (Version 2.06, Keithley, US).<sup>29</sup> The prepared Apt/COF/AAO membrane was installed between two poly-(tetrafluoroethylene) flow cells. Within each cell, an Ag/AgCl electrode was inserted to measure the transmembrane ion current in a transmembrane potential range from  $-1$  to  $1$  V with a scanning rate of  $10$  mV s<sup>-1</sup>. The effective ion-conducting area of the membrane is  $2.5$  mm<sup>2</sup>.  $10^{-5}$  mol L<sup>-1</sup> NaCl solution served as the electrolyte solution. Three replicate measurements were taken for each ion current test.

**Preparation of COF/AAO Membrane.** Amino-functionalized AAO (AAO-NH<sub>2</sub>) was prepared according to Ran et al.<sup>29</sup> The AAO-NH<sub>2</sub> was further used for in situ growth of COF. Briefly, TPB (4.57 mg, 0.013 mmol) and DVA (3.63 mg, 0.020 mmol) were dissolved in 2 mL of *n*-BuOH/THF (3:1, v/v) mixture under ultrasonication. Then, the amino-functionalized AAO membrane was immersed in the aforementioned solution and left to stand at 60 °C for 7 h to obtain amorphous polymer/AAO membrane. The prepared amorphous polymer/AAO membrane was rinsed with ethanol to remove residual solvent and then immersed in the reaction solvent (ACN/12 mol L<sup>-1</sup> acetic acid solution, 50:7, v/v) and incubated at 25 °C for 3 days. Finally, the resulting COF/AAO membrane was washed with THF and ethanol and dried in a fume hood overnight.

**Fabrication of the Apt/COF/AAO Nanofluidic Sensor.** COF/AAO membrane was placed in a three-necked flask. After the flask was vacuumed for 2 h, Tris-HCl buffer solution (10 mmol L<sup>-1</sup>, pH 8.0) containing 500 mmol L<sup>-1</sup> NaCl, 1 mmol L<sup>-1</sup> MgCl<sub>2</sub>, and 1.5 μmol L<sup>-1</sup> Apt was added, and the mixture was reacted for 5 h at room temperature to obtain the Apt/COF/AAO nanofluidic sensor.

**Sample Preparation.** Samples of rice, corn, peanuts, and wheat were procured from local supermarkets (Wuxi, China) and pulverized using a wall breaker. 1 g of the above sample powders before and after spiking was added to 4 mL of ACN/water (8:2, v/v) solution and sonicated for 30 min. The supernatant was then collected through centrifugation at 10,000 rpm for 10 min, adjusted to pH 7.4 with Tris-HCl buffer solution (10 mmol L<sup>-1</sup>, pH 7.4), and filtered through a 0.22 μm membrane. The filtrate was diluted to a volume with ultrapure water in a 5 mL volumetric bottle for subsequent analysis.

**Determination of AFB1.** Typically, Apt/COF/AAO was immersed into a series of standard solutions containing various concentrations of AFB1 (300 μL). After incubation for 40 min, Apt/COF/AAO was rinsed thoroughly with Tris-HCl buffer solution (10 mmol L<sup>-1</sup>, pH 7.4) to obtain AFB1-bound Apt/COF/AAO (Apt/COF/AAO-AFB1). Apt/COF/AAO or Apt/COF/AAO-AFB1 was positioned at the center of the flow cell. Then, 150 μL of electrolyte solution (10<sup>-5</sup> mol L<sup>-1</sup> NaCl) was added to each side of the membrane. *I*-*V* curves were recorded by scanning the voltage in the range -1 to 1 V at a scanning rate of 10 mV s<sup>-1</sup>.

## RESULTS AND DISCUSSION

**Fabrication and Characterization of the Apt/COF/AAO Nanofluidic Sensor.** Figure 1a illustrates the design and fabrication of the Apt/COF/AAO nanofluidic sensor. The amino groups of the AAO-NH<sub>2</sub> membrane first reacted with the aldehyde groups in one COF monomer DVA through the Schiff Base reaction to serve as a bridge between COF and AAO. A two-step approach was then adopted to ensure uniform in situ growth of crystalline COF on the AAO membrane.<sup>46</sup> In step 1, the AAO-NH<sub>2</sub> membrane was immersed in a mixed solution of TPB and DVA to carry out the reaction at 60 °C. This step enabled simple polymerization between the monomers in the absence of a catalyst to ensure the formation of a uniform amorphous polymer layer on the AAO membrane. Step 2 was designed to convert the amorphous polymer grown on the AAO membrane into a crystalline COF layer in ACN under acetic acid catalysis for 3 days. Figure 1b shows the reaction route for the synthesis of

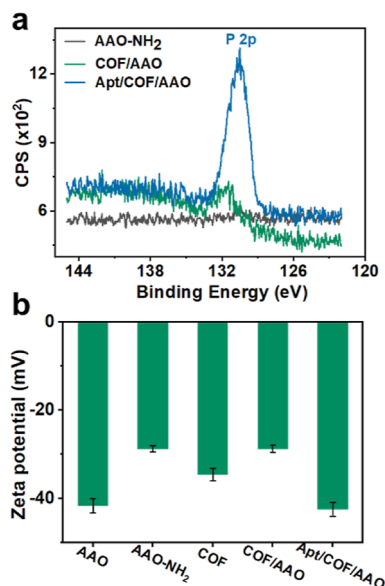
crystalline COF through the two-step method. Furthermore, Apt of AFB1 was introduced as the recognition unit. The aldehyde group of the Apt was covalently bound to the amino groups of TPB on the COF membrane through a Schiff base reaction to construct the Apt/COF/AAO nanofluidic sensor (Figure S1). The specific recognition of Apt toward AFB1 enabled selective alteration in the surface charge of nanochannel to change ionic current. The integration of the high target specificity of Apt with the unique properties of COF makes the developed nanofluidic sensor promising for selective and sensitive detection of trace AFB1 in complex samples. The innovative design not only broadens the application of nanofluidic sensors in the field of food safety but also provides a reference for other fields that require highly selective and sensitive detection techniques.

Uniform distribution and complete coverage of the COF membrane on AAO is crucial for enhancing the performance and reliability of the sensor. Thus, the effect of reaction time on the formation of the COF membrane on AAO nanochannels was studied. The AAO nanochannels were only partially covered by the COF after 24 h of reaction but fully and uniformly covered by the COF membrane after 72 h of reaction (Figure S2). The *I*-*V* curves of nine randomly selected from each of the COF/AAO membrane prepared at different reaction times were tested, and the relative standard deviation (RSD) of the current at -1 V was calculated (Table S1). The results show that 72 h reaction gave the optimal reproducibility. Therefore, 72 h was selected for the preparation of the COF/AAO membrane.

The optimized COF/AAO membrane was characterized by powder X-ray diffraction (PXRD), XPS, scanning electron microscopy (SEM), Fourier transform infrared (FT-IR) spectroscopy, and a N<sub>2</sub> adsorption experiment. The polymer grown on the AAO membrane in step 1 was an amorphous structure (Figure S3). The product from the amorphous polymer in ACN under acetic acid catalysis in step 2 gave the characteristic FT-IR peak of C=N at 1609 cm<sup>-1</sup> (Figure S4), indicating the successful condensation reaction between TPB and DVA to form imine-bonded COF. In addition, the significant PXRD peaks at 2.68, 4.65, 5.41, 7.26, 9.48, and 25.0° (Figure S3), which were in agreement with the simulated peaks of the AA stacking model as well as the reported pattern,<sup>47</sup> confirming the formation of crystalline COF. The intensity of the XPS peak of N 1s in COF/AAO membrane was much stronger than that for AAO-NH<sub>2</sub> due to the contribution of COF (Figure S5). The characteristic diffraction peak at 2.68° and the characteristic IR peak for imine bonds at 1609 cm<sup>-1</sup> appeared in the PXRD pattern and the FTIR spectrum of the COF/AAO membrane, respectively (Figure S6). The above results confirmed the successful growth of crystalline COF on the AAO membrane. Moreover, the crystalline COF grown on AAO was spherical (Figure S7) with about 200 nm thickness (Figure S8), a Brunauer-Emmett-Teller (BET) surface area of 702 m<sup>2</sup> g<sup>-1</sup>, and a pore size of 2.42 nm (Figure S9). The framework of the COF membrane was stable in ambient air and in various organic solvents as well as aqueous solution of acid (1 M HCl) and base (1 M NaOH) (Figure S10).

The Apt/COF/AAO nanofluidic sensor was prepared by grafting Apt on the COF/AAO membrane under the optimal Apt concentration (Figure S11) and reaction time (Figure S12). The as-prepared Apt/COF/AAO nanofluidic sensor gave a distinct characteristic peak of P 2p in the XPS spectra and a

more significant C=N characteristic peak in the FT-IR spectrum, accompanied by the disappearance of the N-H ( $3433$  and  $3353$   $\text{cm}^{-1}$ ) stretching vibrations of TPB on the COF. The above results demonstrated the successful covalent grafting of Apt onto the COF/AAO membrane (Figure 2a;



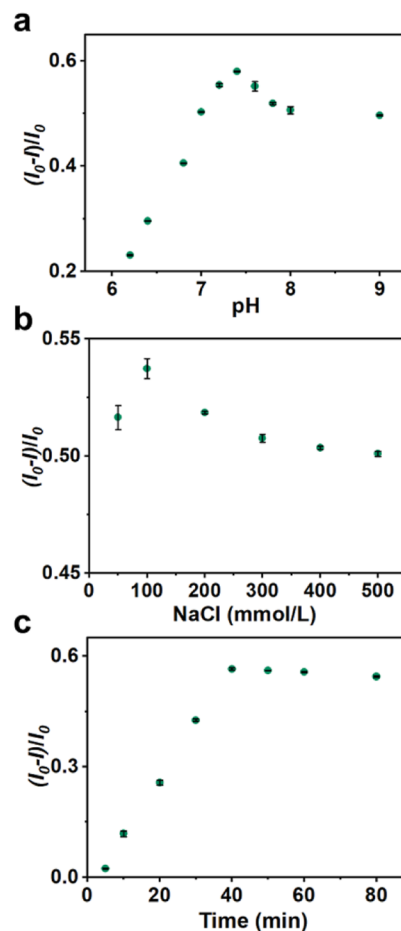
**Figure 2.** XPS spectra of P 2p for AAO-NH<sub>2</sub>, COF/AAO, and Apt/COF/AAO; (b) zeta potentials of AAO, AAO-NH<sub>2</sub>, COF, COF/AAO, and Apt/COF/AAO at pH 7.4.

Figure S13). As shown in Figure S16, both the aptamer and the Apt/COF/AAO sensor gave an isoelectric point (pI) of about 1.5, so the aptamer and Apt/COF/AAO sensor were negatively charged due to the deprotonation of the surface phosphate group at pH > pI. Thus, the as-prepared Apt/COF/AAO exhibited a much negative zeta potential ( $-42.5 \pm 1.6$  eV) than the COF/AAO membrane ( $-28.7 \pm 0.8$  eV) at pH 7.4 (Figure 2b).

**Ion Transport Properties of the Apt/COF/AAO Nanofluidic Sensor.** Surface charge-controlled ion transport is the basis for the Apt/COF/AAO sensor to specifically recognize AFB1. The symmetric transmembrane ion currents verified that the incorporation of COF did not alter the behavior of nanochannel ion transport (Figure S14a).<sup>48,49</sup> Moreover, the ionic transmembrane conductance of the Apt/COF/AAO sensor deviated from the ionic conductance of bulk NaCl electrolyte less than  $10^{-4}$  mol L<sup>-1</sup> (Figure S14b), suggesting that the Apt/COF/AAO sensor was characterized by surface-charge-controlled ionic transport at NaCl concentration less than  $10^{-4}$  mol L<sup>-1</sup>.<sup>50</sup> Therefore, a  $10^{-5}$  mol L<sup>-1</sup> NaCl solution was chosen as the electrolyte for subsequent experiments. In addition, the  $I$ - $V$  curve of the Apt/COF/AAO sensor displayed insignificant change over a four-week period, demonstrating its remarkable stability (Figure S16).

**Sensing Conditions.** To obtain better analytical performance, several important factors such as pH, NaCl concentration, and incubation time were investigated. In order to reflect the performance of the sensor more intuitively, the current reduction rate  $[(I_0 - I)/I_0]$  in the presence of  $100$   $\mu\text{g mL}^{-1}$  AFB1 at  $-1.0$  V, here  $I_0$  and  $I$  refer to the transmembrane ion current before and after adding AFB1, was taken as an indicator for optimization. The current

reduction rate increased to its maximum as the pH increased from 6 to 7.4, gradually decreased with a further increase in pH to 8, and then remained stable over pH 8 (Figure 3a). This is



**Figure 3.** Effect of pH (a), NaCl concentration (b), and incubation time (c) on  $(I_0 - I)/I_0$  in the presence of  $100$   $\mu\text{g mL}^{-1}$  of AFB1 at  $-1$  V.

because pH can affect the charge state of the target and the aptamer through protonation/deprotonation of the carbonyl group in AFB1 (Figure S18) and the phosphate group in the aptamer (Figure S16) to regulate their noncovalent interactions (such as van der Waals, electrostatic, and hydrophobic interactions) and ultimately the changes in current.<sup>51</sup>

The concentration of NaCl can affect the electrostatic interaction between the target and the aptamer. The current reduction rate reached the maximum at a NaCl concentration of  $100$  mmol L<sup>-1</sup> (Figure 3b). In addition, the current reduction rate increased with incubation time up to 40 min and then leveled off (Figure 3c). After incubation for 40 min, the Apt/COF/AAO sensor was rinsed thoroughly with Tris-HCl buffer solution ( $10$  mmol L<sup>-1</sup>, pH 7.4) to remove the unreacted AFB1 residue and eliminate the effect of the high concentration of residual NaCl solution on the surface charge of the sensor. Based on the above results, the following optimal sensing conditions were obtained: pH 7.4,  $100$  mmol L<sup>-1</sup> NaCl, and 40 min of incubation.

**Analytical Performance.** The figures of merit for the developed Apt/COF/AAO nanofluidic sensor for the determination of AFB1 was evaluated under the optimal conditions. Figure 4a shows the  $I$ - $V$  curves at different AFB1

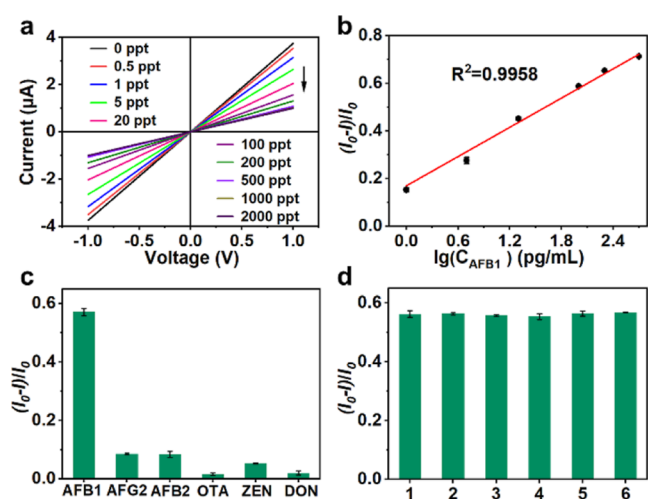


**Figure 4.** (a)  $I$ - $V$  curves of the Apt/COF/AAO nanofluidic sensor for different concentrations of AFB1; (b) calibration curve of  $(I_0 - I)/I_0$  against the logarithm of AFB1 concentration ( $1$ – $500$   $\text{pg mL}^{-1}$ ); (c) effect of AFB1 ( $100$   $\text{pg mL}^{-1}$ ) or other mycotoxins ( $1000$   $\text{pg mL}^{-1}$ ) on the  $(I_0 - I)/I_0$  of Apt/COF/AAO in Tris-HCl buffer solution (pH 7.4); and (d) effects of other mycotoxins ( $1000$   $\text{pg mL}^{-1}$  each) on the determination of AFB1 ( $100$   $\text{pg mL}^{-1}$ ) in Tris-HCl buffer solution (pH 7.4) (1, AFB1 + AFB2; 2, AFB1 + AFG2; 3, AFB1 + OTA; 4, AFB1 + DON; 5, AFB1 + ZEN; and 6, AFB1 + AFB2 + AFG2 + OTA + DON + ZEN).

concentrations. The transmembrane ion current gradually decreased as the AFB1 concentration increased, indicating that the Apt/COF/AAO nanofluidic sensor enables specific binding to AFB1. Moreover, the calibration plot of  $(I_0 - I)/I_0$  against the logarithm of AFB1 concentration was linear in the range of  $1$  to  $500$   $\text{pg mL}^{-1}$  with the linear function of  $(I_0 - I)/I_0 = 0.212 \times \lg C_{\text{AFB1}} + 0.157$  ( $R^2$ , 0.9958) (Figure 4b). The developed Apt/COF/AAO nanofluidic sensor gave a detection limit (3 s) of  $0.11$   $\text{pg mL}^{-1}$ . The relative standard deviation for 11 replicate determinations of AFB1 at  $100$   $\text{pg mL}^{-1}$  was 1.5%. The developed Apt/COF/AAO nanofluidic sensor had a wider linear range and lower detection limit than the Apt/AAO sensor, demonstrating the important role of COF grafting on nanochannels in improving analytical performance (Figure S17 and Table S2). The prepared Apt/COF/AAO nanofluidic sensor also outperforms other methods for AFB1 determination in terms of linear range and detection limit (Table S3), making it a promising detection platform.

To test the selectivity of the developed Apt/COF/AAO nanofluidic sensor, the effect of other mycotoxins (AFB2, AFG2, DON, OTA, and ZEN) on the determination of AFB1 was investigated in the Tris-HCl buffer solution as well as food matrix (rice, wheat, and corn). The structures of the studied mycotoxins are shown in Figure S18. The developed Apt/COF/AAO nanofluidic sensor exhibited high sensitivity to AFB1 but negligible response to other fungal toxins (AFB2, AFG2, OTA, DON and ZEN) (Figure 4c). Furthermore, the addition of interfering mycotoxins at more than 10-fold concentration in a Tris-HCl buffer solution (Figure 4d) and real samples (Figure S19) had almost no effect on the current reduction rate of the proposed Apt/COF/AAO sensor. The recovery of AFB1 ( $100$   $\text{pg mL}^{-1}$ ) spiked into Tris-HCl buffer solution (pH 7.4) ranged between 89.8% and 97.2% in the presence of other mycotoxins ( $1000$   $\text{pg mL}^{-1}$ ) (Table S4).

These results indicate the high specificity of the developed Apt/COF/AAO sensor for AFB1.

**Real Sample Analysis.** The developed Apt/COF/AAO nanofluidic sensor was applied to the analysis of real food samples including wheat, rice, peanuts, and corn for trace AFB1. A certified wheat reference (A299714) was analyzed to confirm the accuracy of the developed sensor. The AFB1 in the certified reference wheat (A299714) was quantified to be  $0.49 \pm 0.02$   $\mu\text{g kg}^{-1}$ , closely matching the certified value of  $0.48 \pm 0.23$   $\mu\text{g kg}^{-1}$ . For the analysis of real samples, AFB1 was detected in both peanut and corn-2 samples with concentrations of  $0.36 \pm 0.10$  and  $0.26 \pm 0.10$   $\mu\text{g kg}^{-1}$ , respectively. In addition, three concentrations of AFB1 ( $1.6$ ,  $8.0$  and  $16$   $\mu\text{g kg}^{-1}$ ) were spiked into each real sample, and the recoveries of AFB1 ranged from 86.9% to 102.5% (Table 1). The results show that the proposed Apt/COF/AAO nanofluidic sensor is promising for the determination of trace amounts of AFB1 in real food samples.

**Table 1. Analytical Results for the Determination of AFB1 in Wheat, Rice, Peanuts, and Corn Samples**

samples	spiked AFB1 ( $\mu\text{g kg}^{-1}$ )	determined AFB1 ( $\mu\text{g kg}^{-1}$ ) (mean $\pm$ s, $n = 3$ )	recovery (%) (mean $\pm$ s, $n = 3$ )
wheat	0	ND <sup>a</sup>	
	1.6	$1.42 \pm 0.05$	$88.8 \pm 3.1$
	8	$7.74 \pm 0.10$	$96.8 \pm 1.3$
rice	0	ND <sup>a</sup>	
	1.6	$1.56 \pm 0.15$	$97.5 \pm 9.4$
	8	$7.74 \pm 0.50$	$96.8 \pm 6.3$
peanuts	0	$0.36 \pm 0.10$	
	1.6	$1.75 \pm 0.03$	$86.9 \pm 1.9$
	8	$8.40 \pm 0.22$	$100.4 \pm 2.8$
corn-1	0	ND <sup>a</sup>	
	1.6	$1.55 \pm 0.07$	$96.8 \pm 4.4$
	8	$7.72 \pm 0.16$	$96.5 \pm 2.0$
corn-2	0	$0.26 \pm 0.02$	
	1.6	$1.82 \pm 0.02$	$97.5 \pm 1.3$
	8	$8.13 \pm 0.08$	$98.4 \pm 1.0$
	16	$15.7 \pm 0.2$	$96.5 \pm 1.3$

<sup>a</sup>ND, not detected.

## CONCLUSIONS

We have developed a nanofluidic sensor for selective and sensitive determination of AFB1 in food samples by integrating the merits of aptamer, 2D COF, and AAO nanochannels. The specific recognition ability of the aptamer and the controlled limited channel space of the COF significantly enhanced the selectivity and sensitivity of the nanofluidic sensor for AFB1 detection. This work has the potential to trigger further exploration in the construction of nanofluidic sensors for the detection of trace contaminants.

## ASSOCIATED CONTENT

### Supporting Information

The Supporting Information is available free of charge at <https://pubs.acs.org/doi/10.1021/acs.analchem.4c04098>.

Methods including instrumentation and preparation of AAO-NH<sub>2</sub>; characterization of COF/AAO membrane synthesized by the two-step method (PXRD, FT-IR, XPS, SEM, and N<sub>2</sub> adsorption); optimization of the initial concentration and reaction time of Apt (UV absorption spectra); *I*–*V* curves of the Apt/COF/AAO sensor determined at different NaCl concentrations; *I*–*V* curves of COF/AAO and Apt/COF/AAO sensors tested at different times; effect of other mycotoxins in the food sample on the  $(I - I_0)/I_0$  of the Apt/COF/AAO sensor; comparison of the sensing performance of Apt/AAO and Apt/COF/AAO; comparison of the developed sensor with others; and determination of the recovery of AFB1 in Tris-HCl buffer solution in the presence of other mycotoxins (PDF)

## AUTHOR INFORMATION

### Corresponding Author

**Xiu-Ping Yan** – State Key Laboratory of Food Science and Technology, Jiangnan University, Wuxi 214122, China; International Joint Laboratory on Food Safety and Institute of Analytical Food Safety, School of Food Science and Technology, Jiangnan University, Wuxi 214122, China; Key Laboratory of Synthetic and Biological Colloids, Ministry of Education, School of Chemical and Material Engineering, Jiangnan University, Wuxi 214122, China; [orcid.org/0000-0001-9953-7681](https://orcid.org/0000-0001-9953-7681); Email: [xpyan@jiangnan.edu.cn](mailto:xpyan@jiangnan.edu.cn)

### Authors

**Shi-Lun Li** – State Key Laboratory of Food Science and Technology, Jiangnan University, Wuxi 214122, China; International Joint Laboratory on Food Safety and Institute of Analytical Food Safety, School of Food Science and Technology, Jiangnan University, Wuxi 214122, China

**Zhu-Ying Yan** – Analysis and Testing Center, Jiangnan University, Wuxi 214122, China; [orcid.org/0000-0002-6818-0728](https://orcid.org/0000-0002-6818-0728)

**Hai-Long Qian** – State Key Laboratory of Food Science and Technology, Jiangnan University, Wuxi 214122, China; International Joint Laboratory on Food Safety and Institute of Analytical Food Safety, School of Food Science and Technology, Jiangnan University, Wuxi 214122, China; [orcid.org/0000-0001-7554-4115](https://orcid.org/0000-0001-7554-4115)

**Shu-Ting Xu** – State Key Laboratory of Food Science and Technology, Jiangnan University, Wuxi 214122, China; International Joint Laboratory on Food Safety and Institute of Analytical Food Safety, School of Food Science and Technology, Jiangnan University, Wuxi 214122, China

Complete contact information is available at:

<https://pubs.acs.org/10.1021/acs.analchem.4c04098>

### Notes

The authors declare no competing financial interest.

## ACKNOWLEDGMENTS

This work was supported by the National Natural Science Foundation of China (nos. 22206060 and 22176073), the Program of “Collaborative Innovation Center of Food Safety and Quality Control in Jiangsu Province”, and the Post-graduate Research & Practice Innovation Program of Jiangsu Province (KYCX24\_2624).

## REFERENCES

- (1) Adunphatcharaphon, S.; Elliott, C. T.; Sooksimuang, T.; Charlermroj, R.; Petchkongkaew, A.; Karoonuthaisiri, N. *J. Hazard. Mater.* **2022**, *432*, 128706.
- (2) Danesh, N. M.; Bostan, H. B.; Abnous, K.; Ramezani, M.; Youssefi, K.; Taghdisi, S. M.; Karimi, G. *TrAC, Trends Anal. Chem.* **2018**, *99*, 117–128.
- (3) Liu, Y.; Wu, F. *Environ. Health Perspect.* **2010**, *6*, 818.
- (4) Sarma, U. P.; Bhetaria, P. J.; Devi, P.; Varma, A. *Ind. J. Clin. Biochem.* **2017**, *32*, 124–133.
- (5) Magnoli, A. P.; Poloni, V. L.; Cavaglieri, L. *Curr. Opin. Food Sci.* **2019**, *29*, 99–108.
- (6) Ismail, A.; Naeem, I.; Gong, Y. Y.; Routledge, M. N.; Akhtar, S.; Riaz, M.; Ramalho, L. N. Z.; de Oliveira, C. A. F.; Ismail, Z. *Trends Food Sci. Technol.* **2021**, *112*, 212–224.
- (7) Bruix, J.; Boix, L.; Sala, M.; Llovet, J. M. *Cancer Cell* **2004**, *5* (3), 215–219.
- (8) Kew, M. C. J. *Gastrointest. Liver* **2013**, *22*, 305–310.
- (9) Wu, F.; Groopman, J. D.; Pestka, J. J. *Annu. Rev. Food Sci. T.* **2014**, *5*, 351–372.
- (10) Rushing, B. R.; Selim, M. I. *Food Chem. Toxicol.* **2019**, *124*, 81–100.
- (11) Hove, M.; Van Poucke, C.; Njumbe-Ediage, E.; Nyanga, L. K.; De Saeger, S. *Food Control* **2016**, *59*, 675–682.
- (12) Vargas Medina, D. A.; Bassolli Borsatto, J. V.; Maciel, E. V. S.; Lanças, F. M. *TrAC, Trends Anal. Chem.* **2021**, *135*, 116156.
- (13) Hamed, A. M.; Abdel-Hamid, M.; Gámiz-Gracia, L.; García-Campaña, A. M.; Arroyo-Manzanares, N. *Anal. Lett.* **2019**, *52*, 363–372.
- (14) Liu, Y.; Liu, D.; Li, C.; Cui, S.; Yun, Z.; Zhang, J.; Wei, Y.; Sun, F. *Crit. Rev. Food Sci.* **2024**, *64*, 5515–5532.
- (15) De Girolamo, A.; Ciasca, B.; Stroka, J.; Bratinova, S.; Pascale, M.; Visconti, A.; Lattanzio, V. M. T. *TrAC, Trends Anal. Chem.* **2017**, *86*, 222–234.
- (16) Zhao, Y.; Wang, X.; Pan, S.; Hong, F.; Lu, P.; Hu, X.; Jiang, F.; Wu, L.; Chen, Y. *Biosens. Bioelectron.* **2024**, *248*, 115992.
- (17) Jia, M.; Liao, X.; Fang, L.; Jia, B.; Liu, M.; Li, D.; Zhou, L.; Kong, W. *TrAC, Trends Anal. Chem.* **2021**, *136*, 116193.
- (18) Bocquet, L. *Nat. Mater.* **2020**, *19*, 254–256.
- (19) Liu, P.; Kong, X. Y.; Jiang, L.; Wen, L. *Chem. Soc. Rev.* **2024**, *53*, 2972–3001.
- (20) Laucirica, G.; Toum Terrones, Y.; Cayón, V.; Cortez, M. L.; Toimil-Molares, M. E.; Trautmann, C.; Marmisollé, W.; Azzaroni, O. *TrAC, Trends Anal. Chem.* **2021**, *144*, 116425.
- (21) Gao, P.; Ma, Q.; Ding, D.; Wang, D.; Lou, X.; Zhai, T.; Xia, F. *Nat. Commun.* **2018**, *9*, 4557.
- (22) Dai, Y.; Zhang, Y.; Ma, Q.; Lin, M.; Zhang, X.; Xia, F. *Anal. Chem.* **2022**, *94*, 17343–17348.
- (23) Wang, J.; Zhou, Y.; Jiang, L. *ACS Nano* **2021**, *15*, 18974–19013.
- (24) de la Escosura-Muñiz, A.; Merkoçi, A. *ACS Nano* **2012**, *6*, 7556–7583.
- (25) Long, Z.; Zhan, S.; Gao, P.; Wang, Y.; Lou, X.; Xia, F. *Anal. Chem.* **2018**, *90*, 577–588.
- (26) Xu, Y.; Li, G.; Xu, W.; Li, Z.; Qu, H.; Cheng, J.; Li, H. *J. Agric. Food Chem.* **2024**, *72*, 11900–11916.
- (27) Zhang, S.; Li, K. B.; Pan, Y.; Han, D. M. *Talanta* **2020**, *220*, 121420.
- (28) Zhang, D.; Zhang, X. *Nano Lett.* **2022**, *22*, 3793–3800.
- (29) Ran, X. Q.; Qian, H. L.; Yan, X. P. *Anal. Chem.* **2021**, *93*, 14287–14292.
- (30) Ran, X. Q.; Qian, H. L.; Yan, X. P. *Anal. Chem.* **2022**, *94*, 8533–8538.
- (31) Guan, Q.; Zhou, L. L.; Dong, Y.-B. *J. Am. Chem. Soc.* **2023**, *145*, 1475–1496.
- (32) Qian, H. L.; Wang, Y.; Yan, X. P. *TrAC, Trends Anal. Chem.* **2022**, *147*, 116516.
- (33) Lu, H.; Wang, C.; Chen, J.; Ge, R.; Leng, W.; Dong, B.; Huang, J.; Gao, Y. *Chem. Commun.* **2015**, *51*, 15562–15565.

- (34) Yu, X.; Li, C.; Chang, J.; Wang, Y.; Xia, W.; Suo, J.; Guan, X.; Valtchev, V.; Yan, Y.; Qiu, S.; Fang, Q. *Angew. Chem. Int. Ed.* **2022**, *134*, No. e202200820.
- (35) Chen, M.; Yang, K.; Wang, J.; Sun, H.; Xia, X.-H.; Wang, C. *Adv. Funct. Mater.* **2023**, *33*, 2302427.
- (36) Li, Z. Q.; Huang, L. Q.; Wang, K.; Xia, X. H. *Acc. Mater. Res.* **2024**, *5*, 761–771.
- (37) Wu, M. Y.; Mo, R. J.; Ding, X. L.; Huang, L. Q.; Li, Z. Q.; Xia, X. H. *Small* **2023**, *19*, 2301460.
- (38) Zhang, S.; Zhou, J.; Li, H. *Angew. Chem., Int. Ed.* **2022**, *61*, No. e202204012.
- (39) Shi, X.; Xiao, A.; Zhang, C.; Wang, Y. *J. Membr. Sci.* **2019**, *576*, 116–122.
- (40) Shi, X.; Wang, R.; Xiao, A.; Jia, T.; Sun, S.-P.; Wang, Y. *ACS Appl. Nano Mater.* **2018**, *1*, 6320–6326.
- (41) Wang, R.; Wei, M.; Wang, Y. *J. Membr. Sci.* **2020**, *604*, 118090.
- (42) Li, L.; Ma, R.; Wang, W.; Zhang, L.; Li, J.; Eltzov, E.; Wang, S.; Mao, X. *TrAC, Trends Anal. Chem.* **2023**, *166*, 117169.
- (43) Tian, R.; Sun, J.; Ye, Y.; Lu, X.; Sun, X. *TrAC, Trends Anal. Chem.* **2024**, *175*, 117710.
- (44) Yang, L.; Yin, X.; An, B.; Li, F. *Anal. Chem.* **2021**, *93*, 1709–1716.
- (45) Yang, L.; Guo, H.; Hou, T.; Zhang, J.; Li, F. *Biosens. Bioelectron.* **2023**, *234*, 115346.
- (46) Deng, W. C.; Qian, H. L.; Yang, C.; Xu, S. T.; Yan, X. P. *ACS Appl. Mater. Interfaces* **2023**, *15*, 54977–54985.
- (47) Ma, W.; Zheng, Q.; He, Y.; Li, G.; Guo, W.; Lin, Z.; Zhang, L. *J. Am. Chem. Soc.* **2019**, *141*, 18271–18277.
- (48) Siwy, Z. S. *Adv. Funct. Mater.* **2006**, *16*, 735–746.
- (49) Jiang, Y.; Feng, Y.; Su, J.; Nie, J.; Cao, L.; Mao, L.; Jiang, L.; Guo, W. *J. Am. Chem. Soc.* **2017**, *139*, 18739–18746.
- (50) Kong, W.; Chen, C.; Chen, G.; Wang, C.; Liu, D.; Das, S.; Chen, G.; Li, T.; Li, J.; Liu, Y.; Li, Z.; Clifford, B. C.; Hu, L. *Small* **2021**, *17*, 2008200.
- (51) Lin, P. H.; Yen, S. L.; Lin, M. S.; Chang, Y.; Louis, S. R.; Higuchi, A.; Chen, W. Y. *J. Phys. Chem. B* **2008**, *112*, 6665–6673.